Hole antidoping of oxides

Oleksandr I. Malyi and Alex Zunger*
Renewable and Sustainable Energy Institute, University of Colorado, Boulder, Colorado 80309, USA

(Received 6 February 2020; accepted 9 April 2020; published 8 June 2020)

In standard doping, adding charge carrier to a compound results in a shift of the Fermi level towards the conduction band for electron doping and towards the valence band for hole doping. We discuss the curious case of antidoping, where the direction of band movements in response to doping is reversed. Specifically, *p*-type antidoping moves the previously occupied bands to the principal conduction band resulting in an increase of band gap energy and reduction of electronic conductivity. We find that this is a generic behavior for a class of materials: early transition and rare-earth metal (e.g., Ti, Ce) oxides where the sum of composition-weighed formal oxidation states is positive; such compounds tend to form the well-known electron-trapped intermediate bands localized on the reduced cation orbitals. What is less known is that doping by a hole annihilates a single trapped electron on a cation. The latter thus becomes electronically inequivalent with respect to the normal cation in the undoped lattice, thus representing a symmetry-breaking effect. We give specific theoretical predictions for target compounds where hole antidoping might be observed experimentally: Magnéli-like phases (i.e., CeO_{2-x} and TiO_{2-x}) and ternary compounds (i.e., $Ba_2Ti_6O_{13}$ and $Ba_4Ti_{12}O_{27}$), and note that this unique behavior opens the possibility of unconventional control of materials conductivity by doping.

DOI: 10.1103/PhysRevB.101.235202

I. INTRODUCTION

Unreactive vs reactive doping. Doping—the release of free carriers in response to chemical substitution—is widely used to convert insulators to metals, thereby instilling conductivity [1,2] to the benefit of designing carrier-transport devices. Doping is particularly useful when it is *unreactive*, i.e., when it just rigidly shifts the Fermi level (E_F) within the doped energy band, which otherwise remains unmodified. In contrast, perturbative or *reactive doping* can involve crystal structural changes (as in the formation of ordered vacancy compounds [3,4] or phase transition upon doping [5,6]), creating doping-induced gap levels (as in Mott insulators [7]), or the formation of Anderson localized bands due to doping-induced disorder [8] all potentially defeating ideal doping action.

Antidoping as a form of reactive doping. An interesting and different example of highly perturbative doping referred to as "antidoping" was recently noted experimentally [9–13] and theoretically [14,15]. For instance, as illustrated in Figs. 1(a) and 1(b), electron antidoping shifts the doped band into the principal *valence* band, instead of the common case of extra electrons shifting E_F towards the conduction band. The electron antidoping was characterized theoretically for Li_xFeSiO_4 [14], Li_xIrO_3 [14], and $SmNiO_3$ [9,10,12–15], where in the first two cases electron antidoping was enabled by Li insertion (lithiation) in these battery systems. Experimental observations also include H/Li doping of $SmNiO_3$ [9,10] and oxygen vacancy doping of $SrCoO_3$ [11]. Such doping [Fig. 1(b)] *increases* the band gap and thus *reduces* the conductivity.

This paper discusses electron antidoping [14] (Sec. II) as a conceptual introduction, giving a new case of $YNiO_3$, exhibiting band gap opening upon *n*-type doping. We then introduce hole antidoping of oxides (Sec. III) explaining the pertinent design principles (Sec. IV) and give specific theoretical predictions (Secs. V–VII) for target compounds where hole antidoping might be observed experimentally. For both electron and hole antidoping, we provide experimentally detectable fingerprints that could aid the identification of this novel form of reactive doping.

II. ELECTRON (*n*-TYPE) ANTIDOPING OF INTERMEDIATE BANDS THAT CONTAIN TRAPPED LIGAND HOLES

Design principles. The type of compounds that can sustain electron antidoping are materials that have in their undoped band structures unoccupied intermediate bands (IBs) containing trapped holes [Fig. 1(a)]. These states can be formed due to anion orbitals that have a less negative formal oxidation state (FOS) than the common FOS of that anion (such as O^{1-} instead of the common O^{2-}, i.e., oxidized anion [16]). The "ligand hole" [7,17] states came into prominence in the context of superconducting compounds where the conduction bands (normally composed of cation orbitals) were found in some cases to be composed of oxidized anion orbitals [18,19] as seen in some bismuthates (i.e., $SrBiO_3$ and $BaBiO_3$), cuprates ($NaCuO_2$), and rare-earth (*R*) nickelate compounds, $RNiO_3$. In some such systems, however, the ligand hole states are a part of an extended conduction band, being spatially delocalized. In contrast, electron antidoping occurs in those compounds where the "ligand hole" bands are isolated in the principal band gap *region* (i.e., not connected by dispersion to the other bands), as illustrated in Fig. 1(a) showing an "empty, *h*-trapped intermediate CB". These *h*-trapped IBs are not defect- or surface-related states, but are proper Bloch-periodic

*alex.zunger@colorado.edu

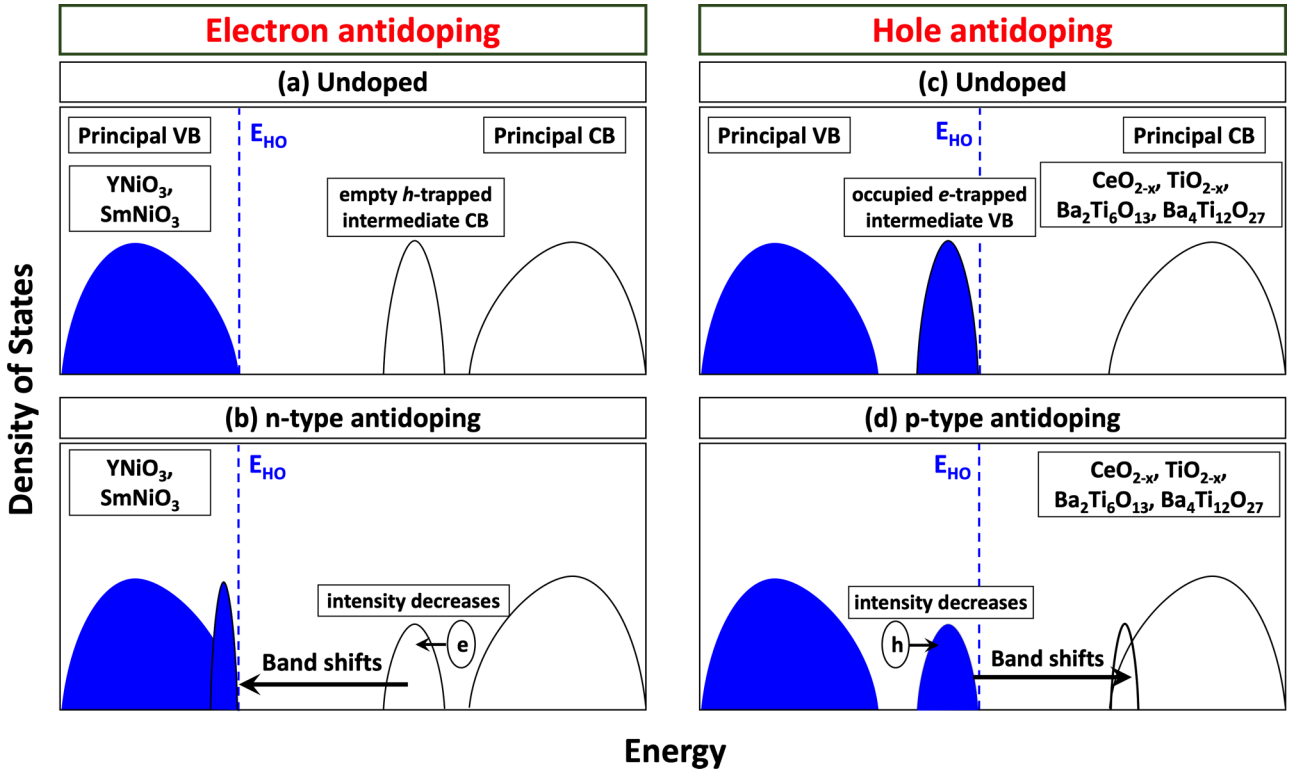

FIG. 1. Schematic illustration of [(a) and (b)] *n*-type and [(c) and (d)] *p*-type antidoping. *n*-type antidoping occurs when adding electrons to unoccupied *h*-trapped in-gap states moves those bands into the principal valence band, resulting in band gap opening. *p*-type antidoping occurs when adding holes to the occupied *e*-trapped in-gap states moves the latter bands to the principal conduction band, resulting in band gap opening. The energy of the highest occupied state (E_{HO}) is shown as a dashed line. The doping induced shift of the intermediate band in (b) and (d) is demonstrated as a progression of in-gap state of reduced intensity. Blue and white regions represent occupied and unoccupied states, respectively. Compounds illustrating these effects are shown in the insets.

eigenstates of the pure host Hamiltonian obtained in band structure calculations, e.g., in Li_xFeSiO_4 [14], Li_xIrO_3 [14], and $SmNiO_3$ [9,10,12–15]. Intermediate bands containing trapped holes are also not necessarily related to any special correlation effect, but exist even in main group s-p compounds such as Mg deficient MgO [14], and are obtainable from routine density functional theory (DFT) calculations featuring exchange-correlation (XC) functionals that are reasonably self-interaction free. While intermediate bands were discussed previously experimentally [20] and theoretically [21–25], here, we focus on the unexplored aspect of doping such intermediate bands. We have previously found that electron antidoping of pristine systems featuring isolated, trapped hole bands leads to the recombination of the resident, trapped hole with the doping electron [14]. This diminishes the intensity of the IB, shifting its intensity to the principal valence band [see the progression of the IB in Fig. 1(b)] while creating a spontaneously broken symmetry state.

Prediction and experimental verification of electron antidoping. To test electron antidoping experimentally, one must first identify a system that has the *h*-trapped IB, as done here or in Ref. [14], and then dope it *n*-type. *n*-type doping of metal oxides can often be done by chemical substitution (e.g., La on Sr [26]), or adding interstitial *n*-type dopants (e.g., Li or H [10,15]), or by the creation of intrinsic donors such as oxygen vacancy [11,13], or facilitating antisite defects of high valent on lower valent cation, as has been demonstrated for a range of systems [27]. To verify electron antidoping once a compound is found one can (i) monitor the *decrease* in intensity of *h*-trapped IBs (e.g., via x-ray absorption spectroscopy or resonant inelastic x-ray scattering) and/or (ii) *increase* of band gap energy and resistivity as the function of *n*-type doping.

A new electron antidoping compound: $YNiO_3$. Using the inverse-design principles for the search of compounds exhibiting electron antidoping [14], one can extend the set of compounds that satisfy the theoretically required conditions of existence empty, *h*-trapped IBs, capable therefore of electron antidoping. For instance, we find here that $YNiO_3$ has an *h*-trapped IB satisfying the electron antidoping principles described in Fig. 1(a). Specifically, according to PBEsol+U calculations (see details on methods in Sec. IV), $YNiO_3$ is S-type antiferromagnetic [28] with a DFT band gap energy of 0.59 eV [Fig. 2(a)]. In the undoped case, the system has two *h*-trapped IBs made of by Ni-d orbitals with a partial contribution of O-*p* states. When doped by $0.5e$/Ni, the population of *h*-trapped IB decreases but no band gap opening is observed. Finally, for $1e$/Ni, band gap opening is observed—the band gap increases from 0.59 to 1.89 eV. The changes in the electronic structure are also reflected in the evolution of partial charge density corresponding to the *h*-trapped IB. Specifically, we observe that the IB in the undoped system has charge localization on both Ni and O ligand states [Fig. 2(b)]. Upon the doping by $1e$/Ni [Fig. 2(c)], the electronically different Ni atoms become alike to each other, and no ligand holes are

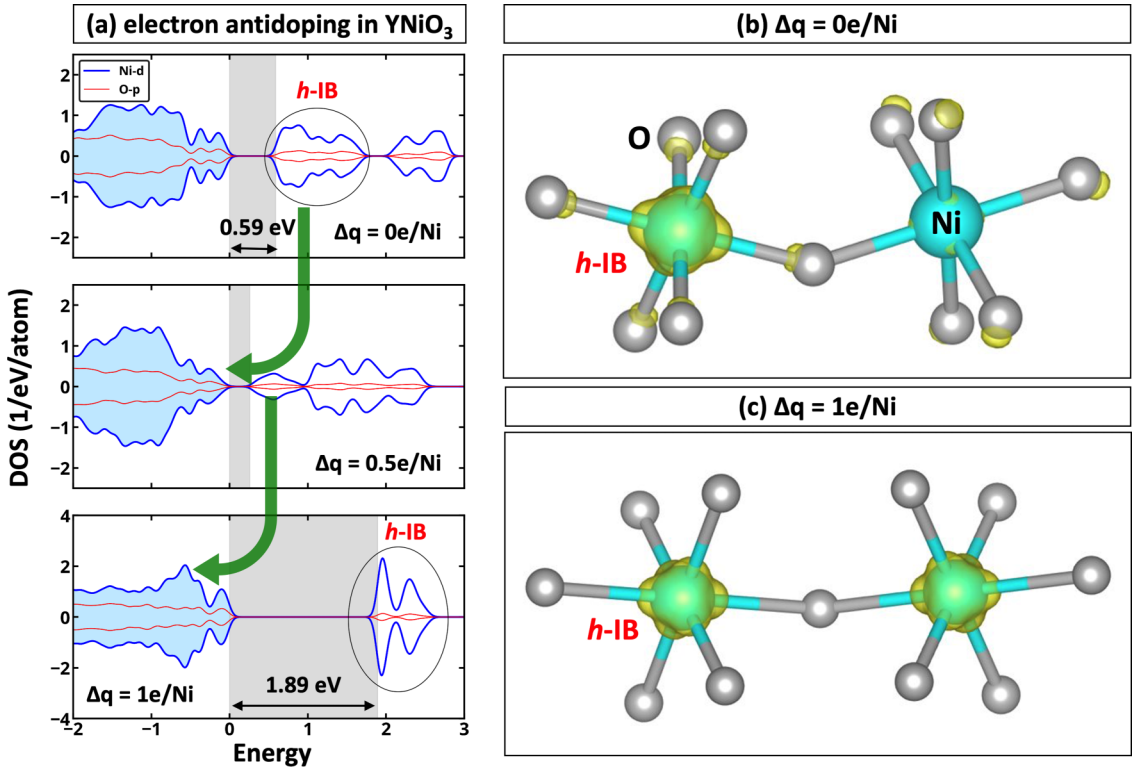

FIG. 2. $YNiO_3$ as a new electron antidoping compound. (a) Density of states for $YNiO_3$ for different electron concentrations computed using PBEsol+U with U value of 2 eV for Ni-d states. The wave function squared of the intermediate state computed over full Brillouin zone is shown in yellow for (b) undoped and (c) $1e$/Ni-doped case. Doping by $0.5e$/Ni shifts the part of the h-trapped intermediate band into the principal valence band. The band gap opening is observed upon doping by $1e$/Ni. The band gap of the system (shown in silver) ranges from the valence band to the lowest energy unoccupied level.

observed. This behavior is similar to that observed for electron antidoping in $SmNiO_3$ [14].

III. HOLE (p-TYPE) ANTIDOPING OF INTERMEDIATE BANDS THAT CONTAIN TRAPPED ELECTRONS ON THE METAL SUBLATTICE

Curiously, despite available data on electron *antidoping* [9–15], missing thus far from the science of quantum materials is the case of "*hole antidoping*" [envisioned in Figs. 1(c) and 1(d)] related to the existence in an undoped host crystal of an isolated, occupied, intermediate *valence* band, associated with *trapped electrons* which, upon *p-type doping* shifts into the principal conduction band (in contrast to the usual case of shifting the doped state into the valence band upon p-type doping). Herein, we search for potential realizations of compounds that could manifest hole antidoping by following the design principles that reflect our physical understanding of the underlying effect.

Design principles. We look for thermodynamically realizable pristine solids (say, with formation energies within less than 15 meV/atom above the convex hull) where the undoped intermediate bands are proper Bloch-periodic eigenstates of the defect- and surface-free compounds and have the following properties: (i) occupied IB, (ii) this IB contains trapped electrons (e-IB), i.e., made of cation orbitals with less positive FOS than the usual. This requires cations that can sustain multiple valences, for instance, Ce^{3+}/Ce^{4+} or Ti^{3+}/Ti^{4+}. (iii) The IB is separated energetically from the principal bands. Indeed, e-IBs are generally composed of reduced cation orbitals and can thus be thought of as being split-off the principal cation-based conduction band. Since generally the energy separation between *localized* cation state (such as electron-trapped band) and the *delocalized* cation conduction band is expected to decrease with increasing atomic number in the periodic table column, herein, we focus on early transition metal and rare-earth (e.g., Ti, Ce) oxides. One should note, however, that the selection of materials used in this work does not exclude the possibility for other compounds to satisfy the design principles described in Figs. 1(c) and 1(d).

We demonstrate that for a range of materials meeting criteria (i)−(iii), for example, the Magnéli-like phases (i.e., CeO_{2-x} and TiO_{2-x}) and ternary compounds (i.e., $Ba_2Ti_6O_{13}$ and $Ba_4Ti_{12}O_{27}$), hole antidoping is robust. Notably, for all considered systems, one hole oxidizes one reduced cation, and hence the band gap opening is only observed when all reduced cations are fully oxidized. This process leads to symmetry breaking, in the sense that electronically equivalent cation sublattices in the undoped compound become electronically distinct after partial hole antidoping. This is the case when doping by a hole annihilates a trapped electron on just a single cation, making this cation now distinct from the other cations.

Prediction and experimental verification of hole antidoping. We distinguish (a) *a priori* conditions for compounds likely to show hole antidoping from (b) *a posteriori* experimental

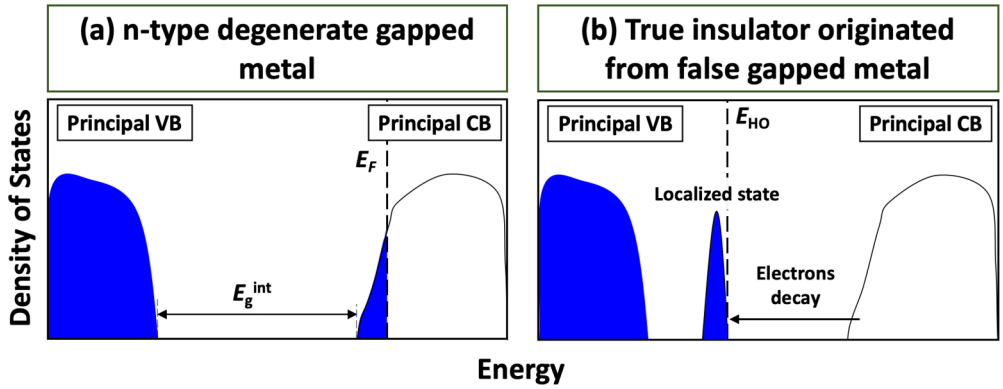

FIG. 3. Schematic illustrations of (a) degenerate gapped metal having electrons in the principal conduction band and an "internal" band gap (E_g^{int}) below the Fermi level and (b) formation of a real insulator from a false degenerate gapped metal due to spontaneous carrier localization resulting in band gap opening. Blue and white regions represent occupied and unoccupied states, respectively.

fingerprints indicating that hole antidoping occurs. For (a), we note the inverse-design principles above. For (b), we list experimental hallmarks of hole antidoping as (i) decrease of intensity of *e*-IB usually on the cation sublattice as a function of *p*-type doping which can be observed by photoemission spectroscopy; (ii) increase of resistivity and band gap as a function of *p*-type doping. From a fundamental perspective, the demonstrated results complement the textbook understanding of doping physics/chemistry, providing the inverse-design principles for developing a new class of materials able to accommodate a large concentration of excessive holes. From an applied point of view, the identification of antidoping could (i) direct future experiments towards studying such exotic doping and (ii) opens the possibility for unconventional control of their electronic properties upon *p*-type doping.

IV. METHODOLOGY

First-principles calculations. For all systems, the spin-polarized calculations are carried out by the Vienna *ab initio* simulation package (VASP) [29–31]. The main calculations are performed using Perdew-Burke-Ernzerhof (PBE) functional [32] with U correction as implemented by Dudarev *et al.* [33] and 4.5 eV U value for both Ce-f and Ti-d states. For electron antidoping, we utilize PBEsol [34] functional with U value of 2 eV applied for Ni-d states, which was suggested by Zunger *et al.* [28] to describe the band gap opening in $YNiO_3$. The used U values are consistent with the available literature [25,28,35,36]. We, however, would like to note that the subject of this paper is on antidoping and not on identifying the U values for specific compounds. The antiferromagnetic magnetic ordering is only considered for compounds containing less than nine metal atoms per primitive cell unless specified. For the selected systems, we also apply revised Heyd-Scuseria-Ernzerhof (HSE) functional [37] calculations to ensure that the results are not affected by the selected methods. Atomic relaxations are carried out only at DFT+U level until the internal forces are smaller than 0.01 eV/Å. The computed results are analyzed using Vesta [38] and pymatgen [39].

Doping calculations. Computationally, nonchemical electron/hole doping is simulated by initially placing the Fermi level at the energetic position that would produce the target doping level, and then nudging the atomic positions as well as charge density so that subsequent atomic force minimization and charge self-consistency lead to a new equilibrium structure. Specifically, for Ce_2O_3, the calculations are performed by doping of both primitive and $3\times3\times2$ supercell sizes. For $Ce_{11}O_{20}$, TiO_{2-x}, $Ba_2Ti_6O_{13}$, and $Ba_4Ti_{12}O_{27}$ polymorphs, the data are presented for primitive cells, but we also ensured that antidoping can be observed for the supercell systems. For electron doping of $YNiO_3$, the calculations are performed for systems ranging from 20- to 80- atom supercell depending on magnetic order. The doping is made for each considered magnetic order; the results are demonstrated for the lowest energy system observed after the doping. One should note that nonchemical doping used in this work has one fundamental difference compared to the chemical doping: the latter involves automatic (chemical) local symmetry breaking (even at low concentration), whereas for nonchemical doping symmetry breaking becomes an option only subsequent to relaxation and self-consistent optimization of the charge density. Despite this, using nonchemical doping allows capturing the main trends for antidoping behavior, as has been illustrated in the example of $SmNiO_3$ [15].

p-type dopability of oxides. Demonstration of hole antidoping requires realization of *p*-type doping, which is generally possible [2,40] when the highest occupied band of a compound is close to vacuum level so that the doped holes do not instigate spontaneous formation of hole killers (such as anion vacancies). It turns out that *e*-IB compounds are ideal candidatures for *p*-type doping satisfying the above doping principle. Specifically, it has been shown that known *e*-IB compounds ($GaTiO_3$, $YTiO_3$, and $LaTiO_3$) have the highest occupied level closer to vacuum level than the systems which do not have *e*-IBs [41]. Moreover, the compounds have been successfully doped *p*-type as has been demonstrated in $GaTiO_3$:Sr [42], $YTiO_3$:Ca [43], and $LaTiO_3$:Sr [44] systems. In addition to the aforementioned chemical doping, one can consider nonchemical doping, e.g., via gating.

Search of candidate compounds for hole antidoping: solids with isolated, occupied, intermediate valence band associated with trapped electrons. Figure 3(a) shows a typical density of states of a metal having E_F in its conduction band and an

internal gap. We refer to this configuration as a "degenerate gapped metal" [3,45]. This can be stable, i.e., it can be real metal as in, e.g., $SrVO_3$ [46] and $Ca_6Al_7O_{16}$ [47] or it can be a "false metal" when the energy lost by creating an occupied band inside the primary gap is less than the energy gained by conduction band electrons decaying into that IB. Use of an XC functional that has good cancellation of self-interaction error (i.e., a "strong functional" with nearly linear total energy versus occupation) manifests relatively compact orbitals that can spontaneously convert the false metal of Fig. 3(a) to a real insulator of Fig. 3(b). On the other hand, the most widely applied XC functional—PBE—(e.g., the one used in Materials Project [48], OQMD [49], and AFLOW [50] open-access materials databases) has a significant "delocalization error," i.e., it tends to overly delocalize states, and the total energy bows down significantly with occupation number [23], thus representing a "soft functional". Such functional is generally not able to stabilize *e*-IB predicting a false metal. This is illustrated in Fig. 4(a) for $LiTi_2O_4$ calculated using the PBE functional, which gives a false metal, whereas utilization of harder functionals [PBE+U, HSE, see Figs. 4(b) and 4(c)] results in an insulator. In fact, more advanced XC functional that can sustain spatially compact orbitals can lower the total energy by expelling an occupied intermediate band to lower energies, inside the fundamental band gap area, breaking symmetry relative to the empty principal conduction band, thus leading to an insulator [Figs. 4(b) and 4(c)]. For instance, in the case of $LiTi_2O_4$, the charge density localization results in spontaneous lowering space group (SG) symmetry from SG = 227 (for PBE) to SG = 15 (for PBE+U and HSE).

We build on this systematic PBE error to identify candidate hole antidoping compounds. To identify insulator compounds whose band structures contain *e*-IBs, we first inspect potential cases of degenerate gapped metals available in Materials Project [48]. Here, we look for band structures of compounds with an odd number of electron/formula unit, that place E_F inside the principal conduction band, making them metals with internal gaps below E_F obtained with soft XC functionals (e.g., PBE). To find such degenerate gapped metals in the database, we seek compounds where the sum of composition-weighed FOS is larger than 0. For example, Ce in CeO_2 has the normal FOS of Ce^{4+}. In Ce_2O_3, assuming this conventional Ce^{4+} FOS, the weighted sum of FOS is positive +2. Similarly, Ti in TiO_2 has the conventional FOS of +4, while $LiTi_2O_4$ has the weighted FOS sum of positive +1. We understand that the FOS does not describe the physical reality of how charge density is distributed around metal sites, simply because a change of charge on a metal site is generally counteracted by opposing changes in the ligands (the "self-regulating response") [51]. We use the FOS strictly as a bookkeeping entity without assigning any physical significance to the charge distribution that they imply. Indeed, in hybridized systems, the physical charge density around metal sites with different FOS is similar to one another [52] as also demonstrated below.

Next, we test which of the found degenerate gapped metals are the false metals, i.e., upon using a stronger XC functional they become true insulators with the split-off state being *e*-IBs localized on reduced cations. This is done by utilizing harder XC functional and analyzing the nature of in-

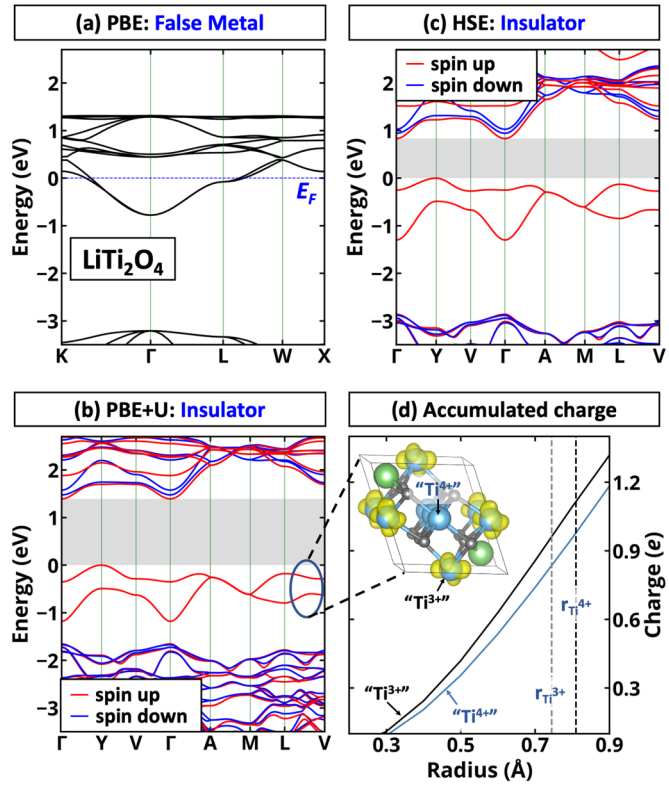

FIG. 4. Symmetry breaking leading to band gap opening in $LiTi_2O_4$. Band structure for $LiTi_2O_4$ computed using (a) PBE, (b) PBE+U, and (c) HSE calculations. PBE calculations predict nonmagnetic metal state, while the PBE+U and HSE calculations localize the charge density leading to the formation of occupied in gap "Ti^{3+}" states and band gap opening. The resulting system is magnetic in both PBE+U and HSE calculations. Red and blue colors represent spin-up and spin-down components. The localization of charge density results in spontaneous lowering symmetry from space group (SG) = 227 to SG = 15. (d) Charge distribution around "Ti^{3+}" and "Ti^{4+}" ions calculated by radial integration of charge density around corresponding Ti atoms. The inset shows in yellow the partial charge density computed over full Brillouin zone corresponding to the *e*-IB for PBE+U calculations. Li, O, and Ti atoms are marked by green, gray, and light blue, respectively. Ionic Ti radii [53] are shown in (d) as vertical dashed lines.

gap states. As an illustration, HSE and PBE+U calculations applied for $LiTi_2O_4$ result in band gap opening [Figs. 4(b) and 4(c)] and electron localization (yellow contours) on part of Ti sublattice as depicted in Fig. 4(d). This more proper treatment of $LiTi_2O_4$ shows an intermediate band in the gap area, resembling an impurity state, except that this band is a strict Bloch periodic state of the perfect host crystal. From the FOS perspective, the symmetry broken phase can be considered as $Li^{1+}Ti^{3+}Ti^{4+}O_4^{2-}$ but, as indicated above, the physical charges around large "Ti^{3+}" and small "Ti^{4+}" sites are rather similar within the relevant ionic radii [53]. The physical difference between the two Ti sublattices is reflected in bond length differences: the average Ti-O distances are 2.12 and 2.02 Å, respectively, for the two sublattices. We show below such wave-function amplitude for other intermediate band compounds studied here, proving localization and

symmetry breaking. In this way, we find many insulators with occupied intermediate bands, which satisfy conditions hole antidoping [Figs. 1(c) and 1(d)]. From the found compounds, e.g., CeO_{2-x}, TiO_{2-x}, A_xCeO_{2-y}, and A_xTiO_{2-y} (A = alkali and alkaline earth metals), we select a few experimentally synthesized representative structures for illustration of the hole antidoping physics.

V. HOLE ANTIDOPING IN CeO_{2-x} LOCALIZES THE CARRIER ON ONE OF THE Ce SUBLATTICES AND SHIFTS THE INTERMEDIATE BAND INTO THE PRINCIPAL CONDUCTION BAND

In-gap trapped electron states in undoped Ce_2O_3. Ce_2O_3 (SG = 164) is an antiferromagnetic insulator which attracted significant attention due to its role in catalysis [54,55]. Its properties (e.g., stability and band gap) have been a subject of detailed investigations by various groups [56–58]. Since the subject of this paper is antidoping, we briefly revisit the basic details on Ce_2O_3 electronic structure to demonstrate that it satisfies the inverse-design principles discussed in Figs. 1(c) and 1(d). At the PBE level, the material is a false degenerate gapped metal with the Fermi level in the conduction band, while using the symmetry breaking XC functional results in band gap opening (the PBE+U band gap energy is 2.68 eV) with the formation of in-gap state containing $2e$/f.u. trapped electrons localized on the two Ce atoms, as shown by the projected density of states [Fig. 5(a)] and wave function squared corresponding to the e-IB [Fig. 5(b)]. It should be noted that the population of the in-gap states for Ce_2O_3 and all other undoped materials discussed below is equal to the composition weighed FOS.

Hole doping of Ce_2O_3 can be unreactive at low concentration. Hole doping of an intermediate band can either (i) keep the carriers delocalized equally on all Ce atoms or (ii) break symmetry. Here, (ii) involves (a) energy lowering localization associated with placing wave-function amplitude on a specific Ce ion, as well as (b) energy raising atomic displacements (i.e., compressing equilibrium bonds). For low hole doping concentration in Ce_2O_3, the energy reduction (a) is smaller than the energy increase needed for breaking local symmetry (b), so no localization occurs according to PBE+U calculations—the Fermi level crosses the e-IB, and the resulted system is the metal with the partially occupied intermediate band. This case corresponds to unreactive doping and is shown in the example of $3\times3\times2$ Ce_2O_3 supercell doped by one hole [Fig. 5(a)].

Concentrated hole doping of Ce_2O_3 moves the intermediate band towards the principal conduction band, resulting in symmetry breaking. While it is understood that, in reality, ultrahigh doping may not be thermodynamically stable (see next paragraph), we use this to illustrate the full trajectory of antidoping. This step is the key to understand if the increase of dopant concentration can make the energy reduction due to hole localization the determining factor and result in the antidoping behavior. This is verified by the hypothetical case of ultra-high doping of Ce_2O_3—adding one hole per primitive cell moves part of the intermediate band to conduction band and makes the two Ce ions inequivalent (disproportionation [52]): one is Ce^{3+}-O^{2-} with larger bond length of 2.42 Å,

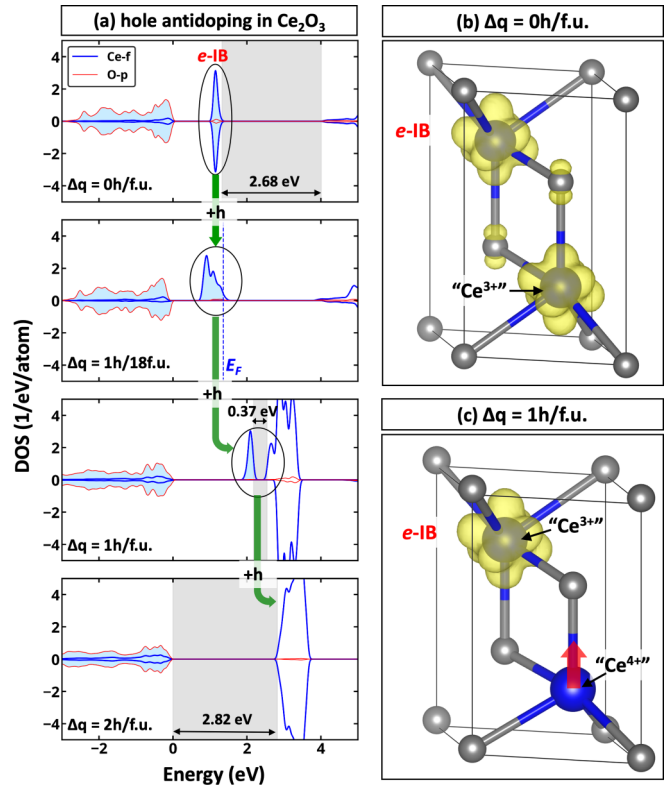

FIG. 5. p-type hole antidoping in Ce_2O_3. (a) Density of states of undoped Ce_2O_3 showing an intermediate band (shown in black) occupied by $2e$/f.u. At low doping ($1h$/18f.u.), the hole is delocalized among all Ce atoms—the doped system is a metal. Doping by $1h$/f.u. converts a single "Ce^{3+}" to "Ce^{4+}" shifting a part of the e-IB towards (depicted by the green arrow) the principal conduction band and causing symmetry breaking (depicted by the red arrow in (c)). Doping by $2h$/f.u. shifts the intermediate band into the principal conduction band resulting in band gap opening. The band gap of the system (shown in silver) ranges from the highest occupied level to the bottom of the principal conduction band. The wave function squared of the e-IB computed over the Brillouin zone is shown in yellow for (b) the undoped case, indicating that it contains a trapped electron on each Ce site; the analogous plot for doping by a single hole is shown in (c) where only one of the Ce atoms shows a trapped electron. O and Ce atoms are marked by gray and blue, respectively.

while the corresponding value for the smaller Ce^{4+}-O^{2-} bond length is 2.32 Å. The resulting system still has the intermediate band occupied by $1e$, which is mainly localized on the large Ce atom [Fig. 5(c)]. Further doping of the system makes the two Ce atoms structurally equivalent to each other and opens band gap—upon doping by $2h$/f.u., the band gap energy of Ce_2O_3 increases from 2.68 to 2.82 eV, as seen in Fig. 5(a).

Hole doping of $Ce_{11}O_{20}$ shifts the intermediate band towards the principal conduction band, resulting in band gap opening. While the case of ultrahigh doping of Ce_2O_3 (Fig. 5) illustrates the full trajectory of antidoping, it may lead to structural instability. To further get the insight into the antidoping of CeO_{2-x}, we examine $Ce_{11}O_{20}$—the experimentally observed phase of reduced CeO_2 [59] consisting of structurally different Ce atoms. According to PBE+U calculations,

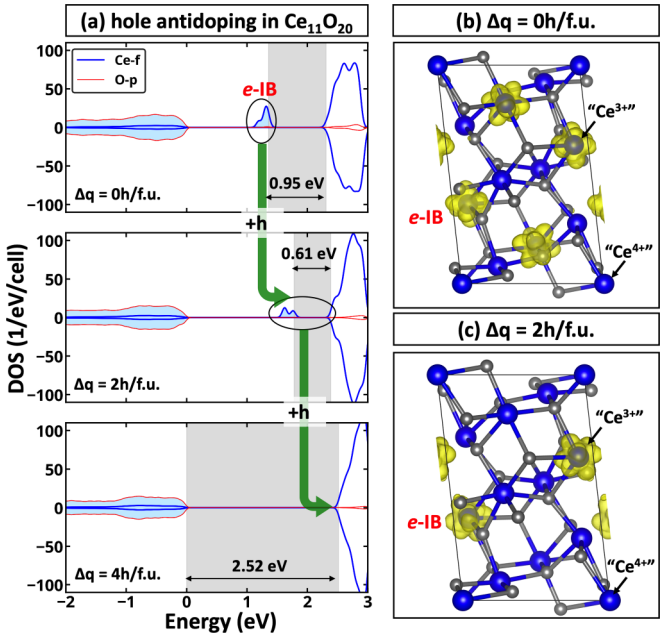

FIG. 6. *p*-type hole antidoping in $Ce_{11}O_{20}$. (a) Density of states of undoped $Ce_{11}O_{20}$ showing an intermediate band (shown in black) occupied by $4e$/f.u. Doping by $2h$/f.u. converts two "Ce^{3+}" to "Ce^{4+}", shifting a part of the intermediate band towards (depicted by the green arrow) the principal conduction band. Doping by $2h$/f.u. further shifts the intermediate band into the principal conduction band resulting in band gap opening. The band gap of the system (shown in silver) ranges from the highest occupied level to the bottom of the principal conduction band. The wave function squared of the IB computed over the Brillouin zone is shown in yellow (b) for the undoped case, indicating that it contains trapped electrons on four Ce sites (isosurfaces localized around four Ce atoms); the analogous plot for doping by $2h$/f.u. is shown in (c) where only two of the Ce atoms have trapped electrons. O and Ce atoms are marked by gray and blue, respectively.

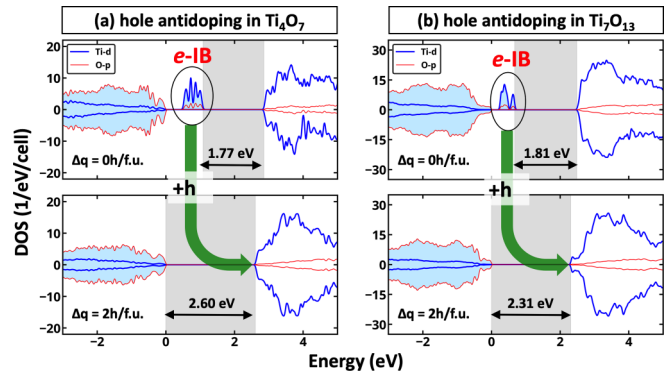

FIG. 7. *p*-type hole antidoping in TiO_{2-x} Magnéli phases. Density of states of (a) Ti_4O_7 and (b) Ti_7O_{13} with different hole concentration (Δq). The band gap of the system (shown in silver) ranges from the highest occupied level to the bottom of the principal conduction band. The intermediate band is made of "Ti^{3+}" states. Adding $2h$/f.u. converts reduced Ti ions, shifting the *e*-IB to the conduction band (depicted by the green arrow) and resulting in band gap opening.

$Ce_{11}O_{20}$ is an insulator with PBE+U band gap energy of 0.95 eV. Here, both the conduction band minimum and the intermediate band are composed of Ce-f states [Fig. 6(a)]—the large "Ce^{3+}" ions determine the occupied intermediate band, while the contribution of small "Ce^{4+}" ions to the *e*-IB is negligible. This is also confirmed by the analysis of charge density corresponding to the *e*-IB suggesting localization of trapped electrons on four large Ce ions, as shown by yellow contours in Fig. 6(b). These results further illustrate the electronically distinct Ce ions with the average Ce^{3+}-O^{2-} and Ce^{4+}-O^{2-} bond lengths of ∼2.49 and ∼2.36 Å. Upon the *p*-type hole doping, the hole is localized on the large "Ce^{3+}" ions resulting in displacing a part the *e*-IB to the primary conduction band—each hole coverts a large Ce to a small Ce atom, reducing the population of the in-gap state [Figs. 6(b) and 6(c)]. Finally, when all reduced Ce atoms are converted (doping by $4h$/f.u.), the local environment for different Ce atoms become similar (the average Ce-O bond length is ∼2.31 Å) and the band gap energy of the system increases from 0.95 to 2.52 eV. Thus these results suggest that *p*-type doping of the Ce-O materials family opens the possibility for unconventional control of materials properties extending the textbook understanding of doping physics/chemistry. Moreover, since the antidoping scenario explains the mechanism of band gap modulation independent on the specific chemical dopant, it allows developing a generic mechanism for modulation of electronic properties upon hole doping.

VI. HOLE ANTIDOPING IN THE MAGNÉLI TiO_{2-x} PHASES LOCALIZES THE CARRIER ON REDUCED Ti ATOMS SHIFTING THE INTERMEDIATE BAND INTO THE PRINCIPAL CONDUCTION BAND

Electron-trapped intermediate band in undoped TiO_{2-x}. The TiO_2 polymorphs [i.e., anatase, rutile, and TiO_2(B)] are wide-gap insulators that have attracted significant attention in photocatalysis [60] and energy storage [61]. Although undoped TiO_2 does not have the in-gap trapped electron state, the compound can be reduced to Magnéli phases (TiO_{2-x})—a family of oxygen-deficient compounds. Similar to *e*-doped TiO_2 polymorphous [25,35,62–64], such phases exhibit the formation of in-gap trapped electron states localized on the reduced Ti atoms [63,64]. For instance, Ti_4O_7 [65] and Ti_7O_{13} [66] are insulators with corresponding PBE+U band gap energies of 1.77 and 1.81 eV and $2e$/f.u. trapped electrons in the in-gap occupied state (Fig. 7). These results are also consistent with the structural analysis—Ti atoms in both structures have 6 nearest O atoms with the average Ti^{3+}-O^{2-} and Ti^{4+}-O^{2-} bond lengths of ∼2.12 and ∼2.02 Å, respectively.

Doped hole localizes on the reduced Ti atoms, moving the intermediate band to the conduction band. Similar to CeO_{2-x}, hole doping of Magnéli TiO_{2-x} phases results in the localization of hole on reduced Ti atoms. Each hole changes one "Ti^{3+}" to "Ti^{4+}", moving the corresponding states to the conduction band. At low doping concentration, this behavior can be seen as a change of the intensity of the *e*-IB, while for large dopant concentration of $2h$/f.u. for which all reduced cations are converted, the band gap opening can be observed.

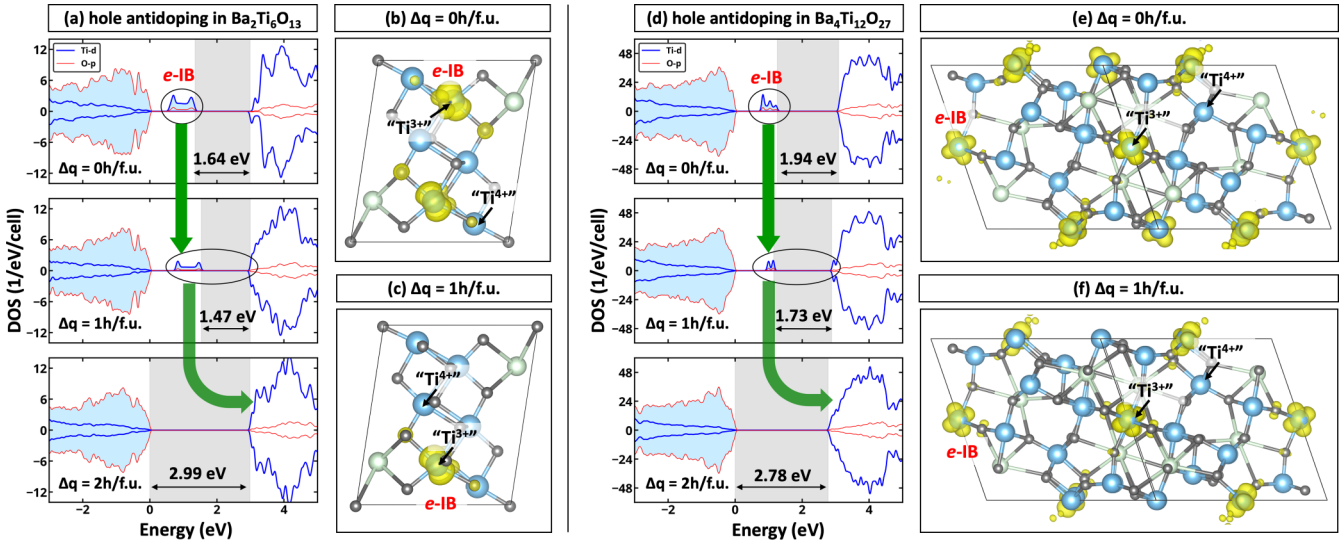

FIG. 8. *p*-type hole antidoping in $Ba_2Ti_6O_{13}$ and $Ba_4Ti_{12}O_{27}$. Density of states of undoped (a) $Ba_2Ti_6O_{13}$ and (d) $Ba_4Ti_{12}O_{27}$ have intermediate bands (shown in black), which are occupied by $2e$/f.u. Doping by hole converts a single "Ti^{3+}" to "Ti^{4+}", shifting a part of the intermediate band towards (depicted by the green arrow) the principal conduction band. Doping by a second hole further shifts the intermediate band into the principal conduction band. The band gap of the system (shown in silver) ranges from the highest occupied level to the bottom of the principal conduction band. The wave function squared of the IB computed over the Brillouin zone is shown in yellow for [(b) and (e)] the undoped case, indicating that it contains trapped electron on Ti sites (iso-surfaces localized around Ti atoms); the analogous plot for doping by $1h$/f.u. is shown in (c) and (f) where only $1e$/f.u. is trapped on Ti atoms. Ba, O, and Ti atoms are marked by light cyan, gray, and light blue, respectively.

As an illustration, the PBE+U band gap energy of Ti_7O_{13} increases from 1.81 to 2.31 eV upon doping by $2h$/f.u. These changes are also reflected in structural changes—the fully doped system has the average Ti-O bond length of ∼2.01 Å similar for all Ti atoms. The conversion of reduced Ti atoms and band gap opening has been recently predicted in other O-deficient TiO_2 [63] upon hole doping confirming the universality of hole antidoping behavior in the reduced TiO_{2-x} systems.

VII. HOLE ANTIDOPING IN $Ba_2Ti_6O_{13}$ AND $Ba_4Ti_{12}O_{27}$ CHANGES "Ti^{3+}" TO "Ti^{4+}" AND MOVES UP THE DOPED BAND INTO THE PRINCIPAL CONDUCTION BAND

Electron-trapped intermediate band in undoped Ba-Ti-O systems. While the CeO_{2-x} and TiO_{2-x} represent a form of reduced oxides, the existence of electronically distinct metal ions can also be observed in ternary compounds. To illustrate this behavior, we consider $Ba_2Ti_6O_{13}$ and $Ba_4Ti_{12}O_{27}$, which have been discussed [67,68] as examples of mixed-valence compounds. Both compounds have the same weighted sum of FOS equal to +2 and are predicted to be degenerate gapped metals at the PBE level. According to PBE+U calculations, $Ba_2Ti_6O_{13}$ and $Ba_4Ti_{12}O_{27}$ are insulators with *e*-IBs and band gap energies of 1.64 and 1.94 eV [Figs. 8(a) and 8(d)], respectively. For both systems, the *e*-IBs are occupied by $2e$/f.u. and localized on part of Ti sublattice [Figs. 8(b) and 8(e)] suggesting the existence of electronically different Ti ions, which can be correlated with the literature discussion on the mixed-valence states (i.e., "Ti^{3+}" and "Ti^{4+}") in the compounds. This is also consistent with structural analysis—although each Ti has the same coordination number (each cation forms six bonds with neighboring O), structurally different Ti ions are observed. The average bond length for Ti^{4+}-O^{2-} is ∼2.02 Å, while the corresponding value for Ti^{3+}-O^{2-} bonds is ∼2.12 Å.

p-type hole doping moves the intermediate band associated with reduced atoms to the conduction band. Upon *p*-type doping of both $Ba_2Ti_6O_{13}$ and $Ba_4Ti_{12}O_{27}$, as shown in Fig. 8, holes localize on "Ti^{3+}" ions moving the part of *e*-IB into the conduction band, thus clearly demonstrating hole antidoping. This is illustrated in the evolution of the projected density of states [Figs. 8(a) and 8(d)] and localization of wave function squared [Figs. 8(b), 8(c), 8(e), and 8(f)] corresponding to the in-gap states. Specifically, adding each hole reduces the population of in-gap states for both materials by $1e$. However, the band gap opening is not observed until all reduced Ti atoms are converted. The fully doped $Ba_2Ti_6O_{13}$ and $Ba_4Ti_{12}O_{27}$ systems (doping concentration of $2h$/f.u.) have the PBE+U band gap energies of 2.99 and 2.78 eV, respectively, which are noticeably larger than those for undoped systems. Hence, these results suggest that adding the holes to the compounds instead of providing free carriers and improving the electronic conductivity provide the opposite effect, which is attributed to the change of oxidation states of the reduced cations. This unusual system's response to doping is also accompanied by structural changes—for the fully doped system, the average bond length for each Ti is in range of 1.99–2.02 Å, which is comparable to Ti^{4+}-O^{2-} bond length in the undoped $Ba_2Ti_6O_{13}$ and $Ba_4Ti_{12}O_{27}$ systems. From a materials science perspective, the found antidoping behavior indicates that controllable hole doping can be used to achieve a target population of the *e*-IB for reaching desired functionality.

VIII. CONCLUSIONS AND DISCUSSION

We demonstrated that compounds having (i) occupied intermediate bands, which are (ii) energetically separated from the principal bands, and (iii) contain trapped electrons made of cation orbitals with less positive FOS (e.g., Ce^{3+}/Ce^{4+} or Ti^{3+}/Ti^{4+}) can exhibit the hole antidoping, i.e., a reactive transfer of intensity of the in-gap states in response to hole doping. The unique response to the doping is governed by local symmetry breaking, which becomes spontaneous when the energy lowering associated with placing wave-function amplitude on a specific metal ion is larger than energy raising due to atomic displacements (e.g., compressing equilibrium bonds) needed for hole localization. This effect is attributed to the ability of early transition and rare-earth metals to change the oxidation states upon doping. Notably, for all considered systems (i.e., CeO_{2-x}, TiO_{2-x}, $Ba_2Ti_6O_{13}$, and $Ba_4Ti_{12}O_{27}$), one hole oxidizes one reduced cation, which results in band gap opening (reduction of electronic conductivity) upon reaching the critical doping concentration. The discovered family of materials opens the possibility for unconventional control of their electronic properties upon *p*-type doping extending the textbook understanding of doping physics/chemistry, especially as the antidoping scenario explains the generic mechanism of band gap modulation independent of the specific chemical dopant. In principles, the phenomena can be verified by measuring the electronic conductivity with respect to hole doping as it has been demonstrated for electron antidoping of $SmNiO_3$ [9,10] or/and monitoring the reduction of the population of *e*-trapped IB (e.g., via photoemission spectroscopy) upon *p*-type doping as it is done for doping of various materials [69] and analysis of in-gap occupied states [70,71] in general.

ACKNOWLEDGMENTS

The work on identifying false metals was supported by the National Science Foundation, Division of Materials Research, Electronic and Photonic Materials program under Grant No. DMR-1806939. The work on doping of quantum materials was carried out within Grant No. DE-SC0010467 from U.S. Department of Energy, Office of Science, Basic Energy Sciences, Materials Sciences and Engineering Division. The authors acknowledge the use of computational resources located at the National Renewable Energy Laboratory and sponsored by the Department of Energy's Office of Energy Efficiency and Renewable Energy. The authors thank Qihang Liu for fruitful discussions.

[1] A. Walsh and A. Zunger, Nat. Mater. **16**, 964 (2017).
[2] A. Zunger, Appl. Phys. Lett. **83**, 57 (2003).
[3] O. I. Malyi, M. T. Yeung, K. R. Poeppelmeier, C. Persson, and A. Zunger, Matter **1**, 280 (2019).
[4] O. I. Malyi, G. M. Dalpian, X.-G. Zhao, Z. Wang, and A. Zunger, Mater. Today **32**, 35 (2020).
[5] G. M. Dalpian and S.-H. Wei, Phys. Rev. Lett. **93**, 216401 (2004).
[6] G. M. Dalpian, Y. Yan, and S.-H. Wei, Appl. Phys. Lett. **89**, 011907 (2006).
[7] M. B. J. Meinders, H. Eskes, and G. A. Sawatzky, Phys. Rev. B **48**, 3916 (1993).
[8] P. W. Anderson, Phys. Rev. **109**, 1492 (1958).
[9] Z. Zhang, D. Schwanz, B. Narayanan, M. Kotiuga, J. A. Dura, M. Cherukara, H. Zhou, J. W. Freeland, J. Li, R. Sutarto, F. He, C. Wu, J. Zhu, Y. Sun, K. Ramadoss, S. S. Nonnenmann, N. Yu, R. Comin, K. M. Rabe, S. K. R. S. Sankaranarayanan, and S. Ramanathan, Nature **553**, 68 (2017).
[10] Y. Sun, M. Kotiuga, D. Lim, B. Narayanan, M. Cherukara, Z. Zhang, Y. Dong, R. Kou, C.-J. Sun, Q. Lu, I. Waluyo, A. Hunt, H. Tanaka, A. N. Hattori, S. Gamage, Y. Abate, V. G. Pol, H. Zhou, S. K. R. S. Sankaranarayanan, B. Yildiz, K. M. Rabe, and S. Ramanathan, Proc. Natl. Acad. Sci. USA **115**, 9672 (2018).
[11] N. Lu, P. Zhang, Q. Zhang, R. Qiao, Q. He, H.-B. Li, Y. Wang, J. Guo, D. Zhang, Z. Duan, Z. Li, M. Wang, S. Yang, M. Yan, E. Arenholz, S. Zhou, W. Yang, L. Gu, C.-W. Nan, J. Wu, Y. Tokura, and P. Yu, Nature **546**, 124 (2017).
[12] J. Shi, Y. Zhou, and S. Ramanathan, Nat. Commun. **5**, 4860 (2014).
[13] M. Kotiuga, Z. Zhang, J. Li, F. Rodolakis, H. Zhou, R. Sutarto, F. He, Q. Wang, Y. Sun, Y. Wang, N. A. Aghamiri, S. B. Hancock, L. P. Rokhinson, D. P. Landau, Y. Abate, J. W. Freeland, R. Comin, S. Ramanathan, and K. M. Rabe, Proc. Natl. Acad. Sci. USA **116**, 21992 (2019).
[14] Q. Liu, G. M. Dalpian, and A. Zunger, Phys. Rev. Lett. **122**, 106403 (2019).
[15] M. Kotiuga and K. M. Rabe, Phys. Rev. Mater. **3**, 115002 (2019).
[16] O. F. Schirmer, J. Phys.: Condens. Matter **18**, R667 (2006).
[17] G. Sawatzky and R. Green, in *Quantum Materials: Experiments and Theory*, edited by E. Pavarini *et al.* (Forschungszentrum Jülich, Jülich, 2016), p. 1.
[18] P. Abbamonte, G. Blumberg, A. Rusydi, A. Gozar, P. G. Evans, T. Siegrist, L. Venema, H. Eisaki, E. D. Isaacs, and G. A. Sawatzky, Nature (London) **431**, 1078 (2004).
[19] A. Khazraie, K. Foyevtsova, I. Elfimov, and G. A. Sawatzky, Phys. Rev. B **97**, 075103 (2018).
[20] D. Emin, *Polarons* (Cambridge University Press, Cambridge, 2012).
[21] F. Iori, M. Gatti, and A. Rubio, Phys. Rev. B **85**, 115129 (2012).
[22] A. Janotti, J. B. Varley, M. Choi, and C. G. Van de Walle, Phys. Rev. B **90**, 085202 (2014).
[23] S. Lany and A. Zunger, Phys. Rev. B **80**, 085202 (2009).
[24] W. H. Sio, C. Verdi, S. Poncé, and F. Giustino, Phys. Rev. B **99**, 235139 (2019).
[25] J. P. Allen and G. W. Watson, Phys. Chem. Chem. Phys. **16**, 21016 (2014).
[26] D. Neagu and J. T. S. Irvine, Chem. Mater. **23**, 1607 (2011).
[27] T. R. Paudel, A. Zakutayev, S. Lany, M. d'Avezac, and A. Zunger, Adv. Funct. Mater. **21**, 4493 (2011).
[28] J. Varignon, M. Bibes, and A. Zunger, Nat. Commun. **10**, 1658 (2019).
[29] G. Kresse and J. Hafner, Phys. Rev. B **47**, 558 (1993).
[30] G. Kresse and J. Furthmüller, Comp. Mater. Sci. **6**, 15 (1996).

[31] G. Kresse and J. Furthmüller, Phys. Rev. B **54**, 11169 (1996).
[32] J. P. Perdew, K. Burke, and M. Ernzerhof, Phys. Rev. Lett. **77**, 3865 (1996).
[33] S. L. Dudarev, G. A. Botton, S. Y. Savrasov, C. J. Humphreys, and A. P. Sutton, Phys. Rev. B **57**, 1505 (1998).
[34] J. P. Perdew, A. Ruzsinszky, G. I. Csonka, O. A. Vydrov, G. E. Scuseria, L. A. Constantin, X. Zhou, and K. Burke, Phys. Rev. Lett. **100**, 136406 (2008).
[35] Y. Zhang, O. I. Malyi, Y. Tang, J. Wei, Z. Zhu, H. Xia, W. Li, J. Guo, X. Zhou, Z. Chen, C. Persson, and X. Chen, Angew. Chem. Int. Ed. **56**, 14847 (2017).
[36] S. Fabris, S. de Gironcoli, S. Baroni, G. Vicario, and G. Balducci, Phys. Rev. B **72**, 237102 (2005).
[37] A. V. Krukau, O. A. Vydrov, A. F. Izmaylov, and G. E. Scuseria, J. Chem. Phys. **125**, 224106 (2006).
[38] K. Momma and F. Izumi, J. Appl. Cryst. **44**, 1272 (2011).
[39] S. P. Ong, W. D. Richards, A. Jain, G. Hautier, M. Kocher, S. Cholia, D. Gunter, V. L. Chevrier, K. A. Persson, and G. Ceder, Comp. Mater. Sci. **68**, 314 (2013).
[40] S. B. Zhang, S.-H. Wei, and A. Zunger, J. Appl. Phys. **83**, 3192 (1998).
[41] L. Bjaalie, B. Himmetoglu, L. Weston, A. Janotti, and C. G. Van de Walle, New J. Phys. **16**, 025005 (2014).
[42] P. Moetakef and T. A. Cain, Thin Solid Films **583**, 129 (2015).
[43] K. Morikawa, T. Mizokawa, A. Fujimori, Y. Taguchi, and Y. Tokura, Phys. Rev. B **54**, 8446 (1996).
[44] T. Yoshida, A. Ino, T. Mizokawa, A. Fujimori, Y. Taguchi, T. Katsufuji, and Y. Tokura, Europhys. Lett. **59**, 258 (2002).
[45] X. Zhang, L. Zhang, J. D. Perkins, and A. Zunger, Phys. Rev. Lett. **115**, 176602 (2015).
[46] L. Zhang, Y. J. Zhou, L. Guo, W. W. Zhao, A. Barnes, H. T. Zhang, C. Eaton, Y. X. Zheng, M. Brahlek, H. F. Haneef, N. J. Podraza, M. H. W. Chan, V. Gopalan, K. M. Rabe, and R. Engel-Herbert, Nat. Mater. **15**, 204 (2016).
[47] S. Matsuishi, Y. Toda, M. Miyakawa, K. Hayashi, T. Kamiya, M. Hirano, I. Tanaka, and H. Hosono, Science **301**, 626 (2003).
[48] A. Jain, S. P. Ong, G. Hautier, W. Chen, W. D. Richards, S. Dacek, S. Cholia, D. Gunter, D. Skinner, G. Ceder, and K. A. Persson, APL Mater. **1**, 011002 (2013).
[49] J. E. Saal, S. Kirklin, M. Aykol, B. Meredig, and C. Wolverton, JOM **65**, 1501 (2013).
[50] S. Curtarolo, W. Setyawan, S. Wang, J. Xue, K. Yang, R. H. Taylor, L. J. Nelson, G. L. W. Hart, S. Sanvito, M. Buongiorno-Nardelli, N. Mingo, and O. Levy, Comp. Mater. Sci. **58**, 227 (2012).
[51] H. Raebiger, S. Lany, and A. Zunger, Nature (London) **453**, 763 (2008).
[52] G. M. Dalpian, Q. Liu, J. Varignon, M. Bibes, and A. Zunger, Phys. Rev. B **98**, 075135 (2018).
[53] R. Shannon, Acta Cryst. A **32**, 751 (1976).
[54] T. Montini, M. Melchionna, M. Monai, and P. Fornasiero, Chem. Rev. **116**, 5987 (2016).
[55] V. Perrichon, A. Laachir, G. Bergeret, R. Fréty, L. Tournayan, and O. Touret, J. Chem. Soc., Faraday Trans. **90**, 773 (1994).
[56] C. Loschen, J. Carrasco, K. M. Neyman, and F. Illas, Phys. Rev. B **75**, 035115 (2007).
[57] S. Fabris, S. de Gironcoli, S. Baroni, G. Vicario, and G. Balducci, Phys. Rev. B **71**, 041102(R) (2005).
[58] P. J. Hay, R. L. Martin, J. Uddin, and G. E. Scuseria, J. Chem. Phys. **125**, 034712 (2006).
[59] E. A. Kümmerle and G. Heger, J. Solid State Chem. **147**, 485 (1999).
[60] A. Fujishima, X. Zhang, and D. A. Tryk, Surf. Sci. Rep. **63**, 515 (2008).
[61] Y. Zhang, Y. Tang, W. Li, and X. Chen, ChemNanoMat **2**, 764 (2016).
[62] A. R. Elmaslmane, M. B. Watkins, and K. P. McKenna, J. Chem. Theory Comput. **14**, 3740 (2018).
[63] A. C. M. Padilha, H. Raebiger, A. R. Rocha, and G. M. Dalpian, Sci. Rep. **6**, 28871 (2016).
[64] A. C. M. Padilha, J. M. Osorio-Guillén, A. R. Rocha, and G. M. Dalpian, Phys. Rev. B **90**, 035213 (2014).
[65] Y. Le Page and M. Marezio, J. Solid State Chem. **53**, 13 (1984).
[66] Y. Le Page and P. Strobel, J. Solid State Chem. **44**, 273 (1982).
[67] D. S. Filimonov, Z. K. Liu, and C. A. Randall, Mater. Res. Bull. **38**, 545 (2003).
[68] A. Currao, Acta Cryst. C **55**, 2 (1999).
[69] Y. Aiura, I. Hase, H. Bando, T. Yasue, T. Saitoh, and D. S. Dessau, Surf. Sci. **515**, 61 (2002).
[70] A. Fujimori, I. Hase, H. Namatame, Y. Fujishima, Y. Tokura, H. Eisaki, S. Uchida, K. Takegahara, and F. M. F. de Groot, Phys. Rev. Lett. **69**, 1796 (1992).
[71] T. Yoshida, M. Kobayashi, K. Yoshimatsu, H. Kumigashira, and A. Fujimori, J. Electron. Spectrosc. Relat. Phenom. **208**, 11 (2016).